ULTRAFINE GRAINED MATERIALS

Room temperature instability of an Al-4%Cu super saturated solid solution in a nano-crystalline alloy produced by SPD

Y. Huang · J. D. Robson · P. B. Prangnell

Abstract The long-term stability of a severely deformed aluminium alloy has been investigated when copper in solution is used to inhibit recovery. A grain thickness of only 70 nm was obtained in an Al-4 wt% Cu alloy, after processing by equal channel angular extrusion to a strain of $\varepsilon_{eff} \sim 15$, resulting in a lamellar nano-grain structure. However, the severely deformed solid solution was found to be unstable at room temperature and copious precipitation of θ occurred at new grain boundaries within the deformed state. The solute level fell to equilibrium within ~ 9 months. The precipitation kinetics were shown to occur at many orders of magnitude higher than can predicted by classical theory.

Introduction

In severe plastic deformation (SPD) processing a steady-state grain size is normally reached at ultra-high strains which limits the level of grain refinement that can be achieved [1, 2]. This limit is controlled by dynamic recovery operating at higher rates than seen under static conditions [1]. As a result, it is difficult to obtain a nano-grain structure in aluminium alloys on SPD processing at room temperature, owing to their relatively low melting point. Methods for decreasing the limiting grain size

include cryogenic deformation [1, 3], pinning boundary migration with particles [4], or the use of solute to inhibit recovery [5, 6]. Of these options, solute is arguably the most effective approach, as cryogenically deformed nano-grained Al-alloys are unstable at room temperature [1] and with particle pinning it is difficult to achieve the required dispersoid densities [4].

Alloying with magnesium has been shown to greatly reduce the grain size in SPD processed aluminium [6–8]. For example, grain widths of ~ 100 nm have been measured in an Al-3 wt% Mg alloy (3.3 at.%), processed to a strain of 10 by equal channel angular extrusion (ECAE) compared to ~ 500–600 nm in very dilute alloys [7]. Mg has long been thought to inhibit dynamic recovery in Al [9] because it reduces the stacking fault energy (SFE) but, the main effect is from the drag of solute atmospheres, as the dissociation of partials is small in Al–Mg solid solutions [10, 11]. Relative to magnesium, the influence of copper on recovery has received less attention. Whilst Cu increases the SFE [12], it has a greater influence on both solid solutions strengthening and reducing the rate of recovery, at least after deformation to conventional strains [10]. For example, in one study grain sizes as fine as ~ 100 nm have been reported in an Al-4 wt% Cu alloy (1.7 at.%) deformed to an effective strain of ~ 9 by ECAE [13], which is lower than that for the same atomic concentration of Mg.

An important consideration in the use of solute to inhibit dynamic recovery and achieve nanograin structures in Al-alloys by SPD is the stability of supersaturated solid solutions. In high pressure torsion ($\gamma \sim 300$) it has been found that Al–Zn solid solutions dynamically decomposed, approaching equilibrium, whereas with Al–Mg only partial decomposition occurred [14]. Straumal et al. explained this difference in terms of the higher diffusivity of Zn, but

Y. Huang · J. D. Robson · P. B. Prangnell (✉)
Manchester Materials Science Centre, The University of Manchester, Grosvenor Street, Manchester M17HS, UK
e-mail: philip.prangnell@manchester.ac.uk

Y. Huang
e-mail: Yan.huang-2@manchester.ac.uk

J. D. Robson
e-mail: Joseph.robson@manchester.ac.uk

found that the overall rate was still 10^8 times faster than for lattice diffusion [14]. The enhanced rate of decomposition was attributed to diffusion being accelerated by the very high vacancy flux produced under SPD conditions, and the sweeping up of solute by the deformation-induced movement of boundaries. Even when dynamic decomposition of supersaturated solid solutions does not occur, several studies have shown that the SPD can increase instability of solid solutions post processing by accelerating precipitation on artificial ageing, which can also change the precipitation sequence [13, 15].

The original objective of this work was to investigate whether a nano-grain structure could be achieved by SPD processing a super saturated Al–Cu solid solution that was finer than that typically seen in Al–Mg alloys, and that remained stable during prolonged service times at room temperature. During the course of this study, it was discovered that the equilibrium Al_2Cu theta (θ) phase precipitated copiously on grain boundaries within the deformation structure on long-term natural ageing after SPD processing. As room temperature precipitation of the θ phase is not normally expected, the present article will focus on quantifying the precipitation kinetics, during natural ageing of a SPD processed Al-4 wt%Cu alloy, with a view to explaining this unusual accelerated ageing behaviour.

Experimental details

A high purity Al-4 wt%Cu alloy (1.7 at.% Cu) was cast in a copper book mould under an argon atmosphere and homogenised at 550 °C for 24 h. The ingots were machined into 100 mm long bars with a 15×15 mm^2 square cross section. The bars were solution treated at 500 °C for 2 h, followed by 4 h at 550 °C, and water quenching, before immediately processing by equal channel angular extrusion (ECAE). ECAE was carried out at room temperature with a ram speed of 50 mm/min, through a 120° die, using colloidal graphite as lubricant. Up to 15 passes were applied to obtain a range of strain levels, using route A [16]; i.e., the specimen orientation was kept constant throughout processing. The effective strain (ε_{eff}) per ECAE cycle was approximately = 0.7 [16]. The deformed specimens were subsequently held at room temperature for up to a year whilst their hardness and microstructures were monitored.

The deformation structures of the ECAE processed billets and the second-phase particles precipitated during natural ageing at room temperature were characterised by backscatter electron (BSE) imaging and electron backscattered diffraction (EBSD) in a high resolution FEI Sirion FEGSEM, fitted with an HKL-EBSD system. This analysis was complemented at higher resolutions in a

Philip CM200 TEM. X-ray diffraction was carried out to confirm the crystal structure of the precipitates. Hardness was measured on an Instron Tukon2100 Vickers microhardness tester, with the application of a 200 g load for 10 s. All the data presented is from near the centre of the longitudinal transverse plane (TD plane) of the ECAE billets, defined by the normal direction (ND) and the extrusion direction (ED). Specimens for SEM-EBSD analysis were mechanically polished to 0.5 μm before electro-polishing in a solution of 30% nitric acid in methanol. TEM thin foils were prepared by jet polishing using the same solution at −30 °C.

Results

The deformed state

Backscatter electron images and EBSD maps in Fig. 1a and b show the deformation structure of the super saturated Al-4 wt% Cu alloy immediately after processing to 15 ECAE passes. The measurement of crystallite sizes from the BSE images was cross-checked using TEM and the results from both techniques were in good agreement. After deformation to an effective strain of 10, the average crystallite size was only 65 nm wide by ∼500 nm long. This is similar to the value of ∼100 nm reported by Murayama et al. for an alloy of similar composition after ECAE processing [13], and is smaller than that observed in an Al-3.3 at.% Mg alloy deformed under identical conditions [7], confirming the greater effectiveness of Cu in reducing the grain size during SPD processing. In the EBSD maps the average lamellar HAGB spacing was measured to be $\lambda_{ND} = 80$ nm, which confirms that the lamellar boundaries were predominantly high angle in character. However, it can be seen that some of the lamellar grains extend over several microns and the average length, or HAGB spacing in ED, was estimated to be $\lambda_{ED} \sim 1$ μm, giving a grain aspect ratio of ∼13–15 after processing. Therefore, whilst it is possible to obtain much finer deformation structures by using solute to inhibit recovery in SPD, with directional deformation processes the resultant grain structures tend to be highly elongated and contain thinner, much higher aspect ratio grain fragments. Such ultra-high strain deformation structures thus only approach the nano-scale in the transverse direction.

Accelerated precipitation in the severely deformed samples

In Fig. 2 the natural ageing response of samples processed to 5 and 15 ECAE passes are compared to a solution-treated undeformed control on natural ageing at ∼20 °C

Fig. 1 Electron backscatter image (**a**) and EBSD map (**b**) of the Al–4Cu sample, showing the grain structure size after processing by 15 ECAE passes and the second-phase particles within the deformation structure that develop on natural ageing at room temperature for (**c**) 21 days, (**d**) 45 days, and (**e**) 180 days; (**f**) the solution treated un-processed material after 300 days for comparison
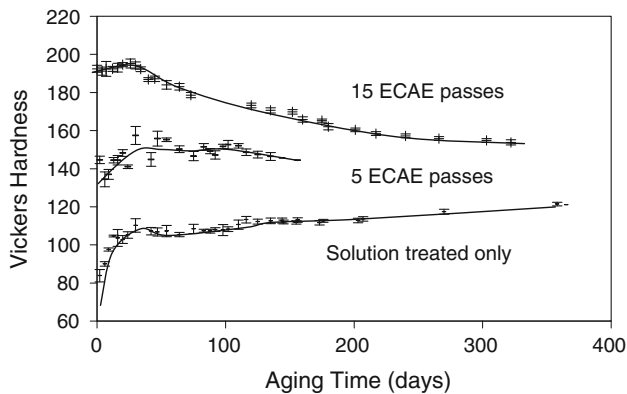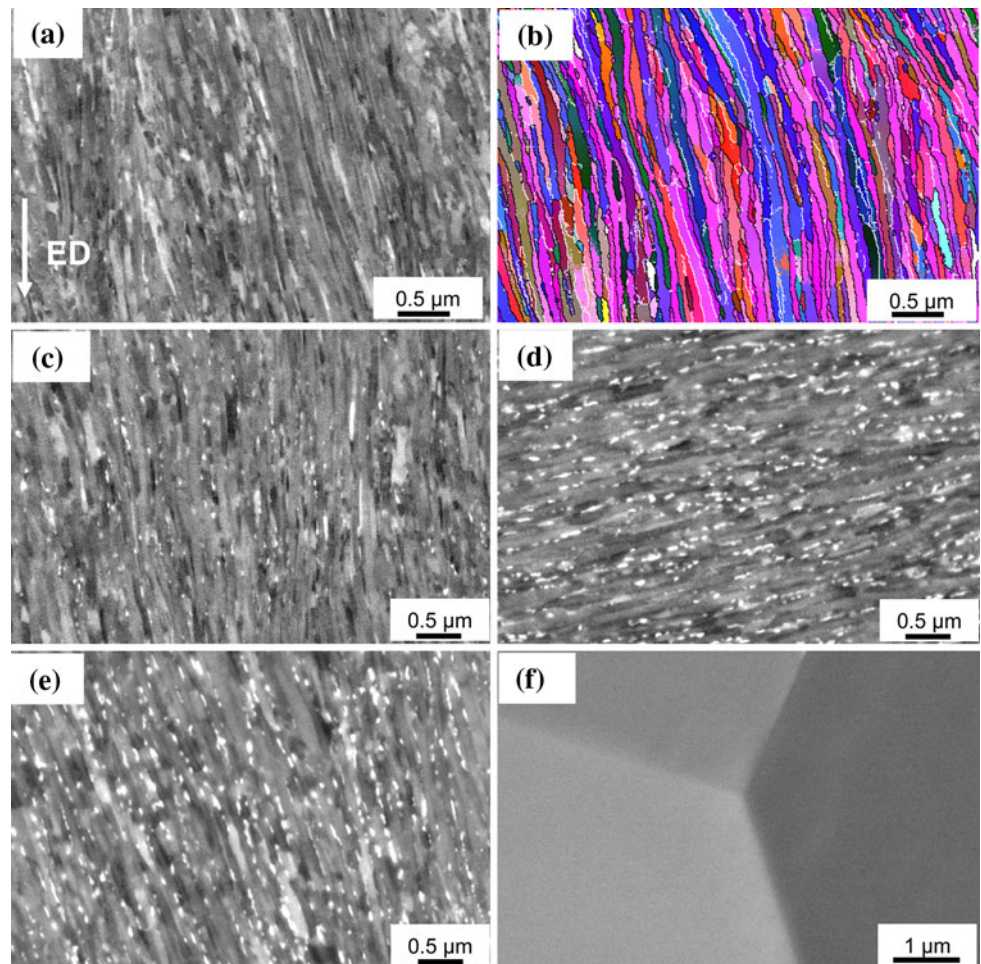

Fig. 2 Natural ageing curves (at $\sim$20 °C) for samples, undeformed, and following processing by ECAE to a total of 5 and 15 passes

(192 HV) which only initially increased very slightly before decreasing gradually with time.

Microstructural analysis (Fig. 1) revealed that this decrease in hardness was associated with fine-scale precipitation starting to occur on grain boundaries within the ECAE processed materials after three weeks. In contrast, no evidence of room temperature grain boundary precipitation was seen in the undeformed solution-treated alloy even after natural ageing for up to a year (Fig. 1f). All the precipitates were found to have nucleated on grain boundaries, and with increasing ageing time, their number density and size progressively increased. X-ray diffraction revealed only the presence of the equilibrium θ phase in the naturally aged ECAE processed samples. No evidence of GP zones, or θ'' and θ' precipitates could be identified in TEM images, or from selected area diffraction.

Kinetic data

The half length (L), half width (r), number density and volume fraction of θ precipitates with natural ageing time were measured from TEM and BSE images and are shown

for up to one year. As expected, on natural ageing the hardness of the undeformed, as-solution treated, sample rose rapidly from 84 to 104 HV in two weeks and then continued to increase at a slower rate as ageing continued, reaching a value of 121 HV after 12 months. In contrast, the material processed to a strain of $\varepsilon_{\mathrm{eff}} \sim 10$ exhibited a much higher hardness immediately after ECAE processing
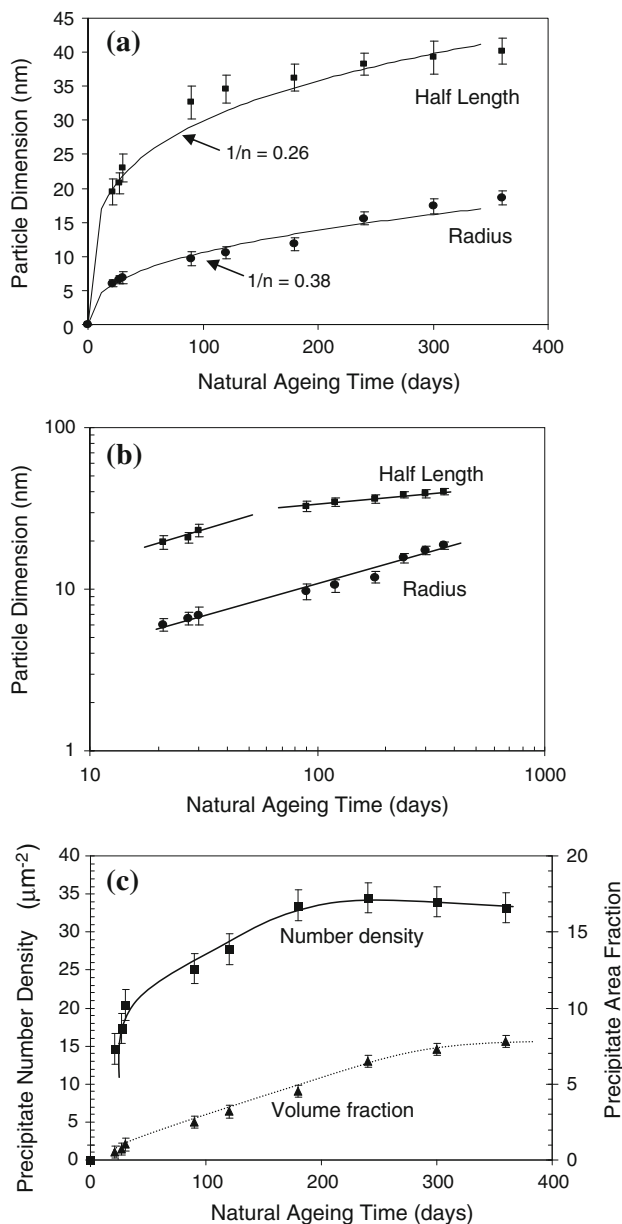
Fig. 3 (**a**) Measurements of θ precipitate dimensions (radius r, and half length L) from the sample subjected to 15 ECAE passes, as a function of natural ageing time, (**b**) re-plotted logarithmically showing evidence of two slopes with, $1/n \sim 0.35$ and $1/n \sim 0.14$ for the precipitate half-length results. (**c**) The precipitate number density and volume fraction with natural ageing time. In (**a**) the continuous lines are fitted curves with $t = k_1 r^{0.38}$ and $t = k_2 L^{0.26}$

in Fig. 3. It can be seen from Fig. 3a that the precipitate dimensions increase at a diminishing rate with time, but after one year their average width and length had increased to 37 and 80 nm, respectively. Linear regression fits to all the data, when plotted logarithmically (Fig. 3b), gave exponents of $r^{0.38}$ and $L^{0.26}$, which is in close agreement with the $t = k_2 r^{1/2}$ and $t = k_1 L^{1/4}$ relationships originally proposed by Aron and Aaronson for their collector plate

theory [17] and the results therefore, follow the expected behaviour for diffusion controlled grain boundary growth. However, due to the close spacing of the precipitates within the boundary plane and simultaneous recovery of the deformation structure, the behaviour is not as straight forward as this simple fit implies. In Fig. 3b it can be noted that the lengthening results shows evidence of two slopes, the first implying $1/n \sim 0.35$ and the second $1/n \sim 0.14$.

The area fraction and number density of the θ precipitates with time are also given in Fig. 3c, where it can be seen that both parameters approach a constant level after ~ 9 months. This suggests that the solute super saturation has decayed and approached the equilibrium concentration. The area fraction of the θ phase at steady state was $\sim 7\%$ which, given the uncertainty in the measurements, is consistent with an equilibrium volume fraction predicted from thermodynamic calculations of $\sim 5\%$ [18].

θ precipitation was also found to form during natural ageing in the samples processed by ECAE to lower strains. Even in the sample processed by 2 ECAE passes, following 4 months natural ageing at room temperature, θ precipitates were found locally within intense shear bands, where new deformation-induced high angle boundaries were observed (Fig. 4a). It was apparent that the precipitation kinetics were directly related to the density and character of the boundaries generated during ECAE processing. An example of this behaviour can be seen from the higher magnification image of θ boundary precipitation in Fig. 4b where the misorientation of individual boundaries are shown.

Discussion

Under the extreme strain levels reached in SPD dynamic precipitation is not unexpected [14]. However, the observations reported here are solely related to the acceleration of static precipitation by prior severe deformation. Precipitation of the θ phase in Al–Cu alloys at specific sites such as grain boundaries has been only previously observed [17, 19–21] at temperatures greater than 170 °C. The one exception to this research are the results of Murayama et al. [13] who, on ageing an equivalent alloy at 100 °C, also noted θ precipitation at grain boundaries after ECAE processing to a similar strain level. Murayama et al. further showed that the metastable transition phases normally seen on ageing Al–Cu alloys did not form in the SPD processed material, due to the high-nucleation site density for θ precipitation. A similar behaviour to that reported by Murayama et al. [13] was thus seen in the current work, but over a longer time scale at room temperature, with the solid solution decaying directly by the formation of θ bypassing the normal transition phase sates.

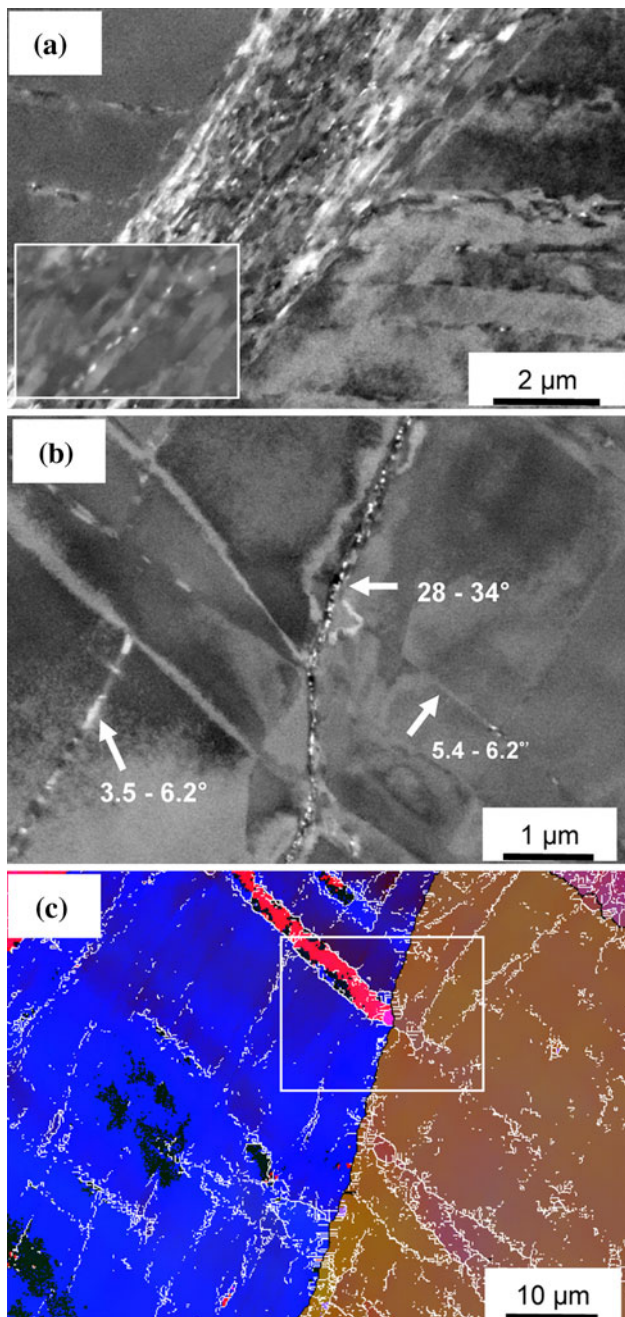**Fig. 4** (**a**, **b**) Electron backscatter images obtained from samples naturally aged at room temperature for 4 months after ECAE processing to two passes; showing the dependence of the precipitation behaviour on the heterogeneity of the deformation structure; in (**b**) at a higher magnification with the misorientation of specific boundaries identified (*arrows*) from the EBSD map in (**c**)

Grain boundary nucleation of the θ phase at room temperature

Heterogeneous nucleation on grain boundaries is classically described in terms of the reduction in energy barrier that results from destruction of grain boundary area, when
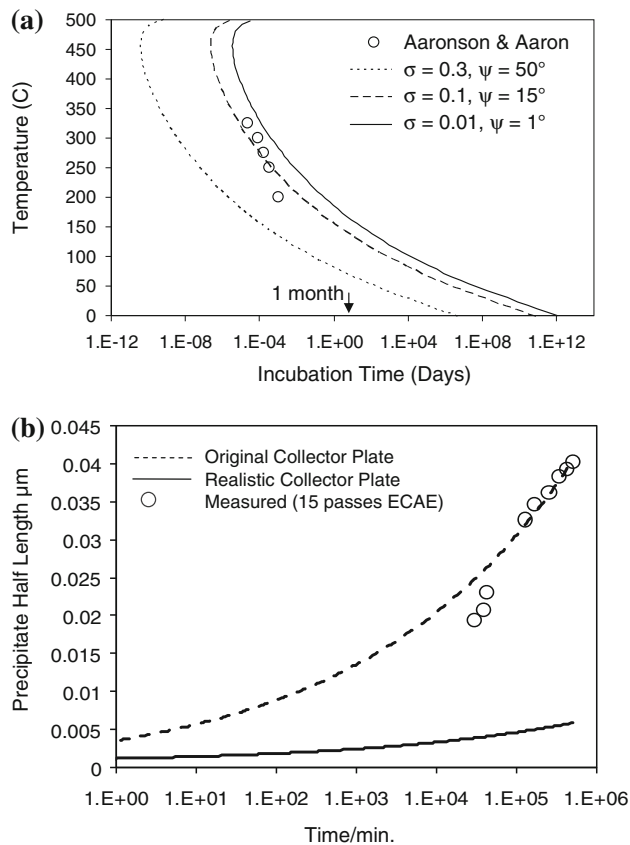

Fig. 5 (**a**) Predicted incubation times for θ precipitates from classical nucleation theory for three different nucleus interfacial energy (σ) and contact angles (ψ) compared to the measured data of Aaron and Aaronson [17]; in (**b**) the half length of grain boundary nucleated θ estimated by collector plate theory as a function of time at room temperature (20°), using different assumptions explained in the text

the boundary plane is wetted by the nucleus [17]. Here we have used classical theory to make ballpark estimates of grain boundary nucleation times expected for the θ phase, in order to identify the factors that control the observed accelerated nucleation rate. Following Russell [20], for a cap-shaped nucleus geometry, the incubation time for nucleation (τ) is given by:

$$\tau = \frac{kT\sigma_{\alpha\theta}a^4}{V_\alpha^2 \Delta G_v^2 D_v \bar{c}} \frac{(2 - 3\cos\psi + \cos^3\psi)}{(1 - \cos\psi)} \tag{1}$$

where k is Boltzmann's constant, T is absolute temperature, $\sigma_{\alpha\theta}$ is the interfacial energy of the nucleus/matrix interface, a is the matrix lattice parameter, V_α is the atomic volume of the copper solute, ΔG_v is the volume free energy change for formation of θ, D_v the diffusion coefficient of copper in the aluminium matrix (given by [22]), $\bar{c}$ the mole fraction of solute in the matrix and ψ the nucleus contact angle.

In Fig. 5a, Eq. 1 has been applied to estimate the expected incubation time at room temperature (20 °C) using various assumptions about the nucleus shape and interfacial energy. Also plotted on this figure are the

measured incubation times of Aaron and Aaronson [17, 20]. The first assumptions used are the same as that by Brailsford and Aaron [23] where it was assumed that the contact angle (ψ) and interfacial energy ($\sigma_{\alpha\theta}$) for the nucleus are the same as those for growing θ precipitates ($\psi = 50°$, $\sigma_{\alpha\theta} = 0.3$ Jm^{-2}). Using these values predicts the longest incubation times (rightmost curve) in Fig. 5a. For room temperature ageing, this gives an estimated incubation time for grain boundary nucleation of 7.5×10^7 years.

Reducing the interfacial energy to 0.2 Jm^{-2} would require $\psi = 15°$ to maintain equilibrium. Using these parameters produced the middle curve, and gives a more reasonable fit to Aaron and Aaronson's incubation times measured at above 250 °C. However, when the curve is extended to room temperature ageing, the predicted incubation times still remain far too long ($\sim 1.4 \times 10^6$ years) to explain the measured nucleation kinetics. If very low values are used for the interfacial energy and wetting angle (e.g. $\sigma_{\alpha\theta} = 0.01$ Jm^{-2}, $\psi \sim 1°$) a much shorter incubation time is predicted (left hand curve in Fig. 5a). Nevertheless, even with this extremely favourable set of conditions, the incubation time at room temperature is still predicted to be in excess of 80 years, whereas in practice small precipitates were observed after less than a month in the severely deformed material.

The above analysis thus demonstrates that at low temperatures, the incubation time is dominated by the low diffusion coefficient term in Eq. 1. An additional factor that could accelerate nucleation is a higher copper content in the grain boundaries, caused by forced migration of boundaries during deformation which could result in stronger copper segregation from the swept matrix, increasing the driving force and local availability of solute. However, more important, given the dominance of mobility over the driving force, is the strong possibility of diffusion being enhanced by contributions from the high initial deformation-induced vacancy concentration [24] and the more disordered nature of the boundaries in the SPD processed material [25]. A temporary 10^6 rise in vacancy content, is consistent with that expected immediately after severe deformation [24], and could produce an increase in mobility sufficient to explain how room temperature nucleation is possible, even when using the more realistic second set of assumptions detailed above. Although the vacancy concentration will rapidly decay, this is probably still the most significant factor encouraging nucleation in the SPD processed material, as predictions of the nucleation rate retain large levels of uncertainty and PALS measurements show that the excess vacancies will survive, all be it at a reducing level, over a similar period to that required for the first precipitates to become visible [26].

Room temperature growth kinetics

A number of models exist describing the growth rate of grain boundary nucleated phases that follow on from the original pioneering work by Aaron and Aaronson [17]. Here we have used a version of the theory with a constant collector plate area, as proposed by Carolan and Faulkner [27], to estimate the expected growth rates of the θ phase at room temperature, from:

$$\frac{dL}{dt} = \frac{A_v \sqrt{D_v} (\bar{x} - x_r^{\alpha\theta})}{3\pi^{3/2} f(\psi) (x^\theta - x_r^{\alpha\theta})} \frac{\sqrt{t}}{L^2} \qquad (2)$$

where A_v is the collector plate area, $\bar{x}$ the volume fraction of copper in the matrix, $x_r^{\alpha\theta}$ the volume fraction of copper at the precipitate/matrix interface corrected for curvature (the Gibbs–Thompson effect), x^θ the volume fraction of copper in the precipitate, $f(\psi)$ a geometric factor (the expression for which is given in [27]), L the precipitate half-length and t time.

Surprisingly, using identical input parameters to those adopted by Brailsford and Aaron [23] if Eq. 2 is extrapolated to 20 °C without any modification to the input parameters, it fits our results for the severely deformed material remarkably well, particularly at longer times (Fig. 5b). However, the input parameters are unrealistic for the severely deformed alloy. In particular, the collector plate area is determined by the precipitate spacing on the grain boundary, and this is much smaller in our work than in that of Aaron and Aaronson [17]. A more realistic assessment of the collector plate size based on the actual measured interparticle spacing and a more recent assessment of the diffusion coefficient [22] gives greatly reduced predicted growth kinetics, as shown in Fig. 5b (solid line). With this more appropriate set of input parameters the predicted precipitate size, according to Eq. 2, is now about eight times smaller than that measured. However, this discrepancy is not as large as the factor of $\sim 10^6$ estimated for the nucleation kinetics, which clearly explains why θ would not normally be seen on natural ageing an undeformed alloy, even if there was no growth limitation.

Whilst not as dramatic as the influence of SPD on room temperature nucleation rates, this again implies that factors not accounted for in classical theory must be important in accelerating growth kinetics of grain boundary nucleated phases in heavily deformed materials. Although it can be argued that the deformation-induced excess vacancy concentration is important in providing sufficient atomic mobility to contribute to nucleation, the decay rate of even a large non-equilibrium vacancy concentration will be too short [26] to have much impact on growth occurring over a one-year time scale. In the collector plate theory [27] it is assumed that grain boundary diffusion is infinitely rapid

relative to diffusion to the boundary and the dominant factors are the movement of solute to the boundary and the size of the collector plate. The size of the collector plate is relatively small in a severely deformed alloy, and the rate determining step therefore is the supply of solute to the boundaries. It is possible this could be enhanced by two factors. Firstly, dislocations attached to boundaries, that extend into the matrix could assist in supplying solute, although this effect would diminish as recovery occurs. Secondly, as some migration of the lamellar boundaries occurred simultaneously with θ precipitation migration of segments of HAGBs, between pinning points from second phase particles could sweep copper atoms to boundaries enhancing the collector plate effect. The possibility of a greater supply of solute caused by slowly migrating grain boundaries is not accounted for in the simple classical growth model and, although the potential influence of this effect requires further investigation, it is likely to be a key factor contributing towards the acceleration of the room temperature θ growth kinetics in the SPD processed material.

Conclusions

The grain size achievable after SPD processing and long-term stability of an aluminium copper alloy has been investigated. After deformation to a strain of $\varepsilon_{eff} \sim 10$, by ECAE through 'route A', the deformed state contained highly elongated lamellar grain fragments with a grain width of only 70 nm and an average length of $\sim 1\ \mu m$. This compares to a grain width of 150 nm for an identically processed 3 wt% Mg alloy, which contained double the atomic concentration of solute.

Post-ECAE processing, the severely deformed Al–Cu solid solution was found to be unstable at room temperature and precipitation of θ occurred at grain boundaries on natural ageing. Precipitation of GPZs, or the other transition phases, was not observed and the solute level fell to equilibrium within ~ 9 months.

Analysis showed that nucleation of θ was only possible in the severely deformed alloy, due to enhanced diffusion accelerated by the high-initial vacancy flux. In comparison, the excess vacancy concentration would not be expected to survive for sufficient time to have a great impact on the growth kinetics. Estimates of the growth rate of the θ precipitates, using collector plate theory, predicted particle sizes an order of magnitude smaller than observed. It is suggested that room temperature growth of the Θ phase in the SPD processed alloy was assisted by the migration of HAGBs during recovery, sweeping copper atoms to the boundaries.

References

1. Huang Y, Prangnell PB (2008) Acta Mater 56:1619
2. Hebesberger T, Stüwe HP, Vorhauer A, Wetscher F, Pippan R (2005) Acta Mater 53:393
3. Zahid GH, Huang Y, Prangnell PB (2009) Acta Mater 57:3509
4. Prangnell PB, Berta M, Apps PJ, Bate PS (2004) In: Bacroix B et al (eds) 2nd International conference on recrystallisation and grain growth, Annecy, France, p 1261
5. Zhao YH, Zhu YT, Liao XZ, Horita Z, Langdon TG (2007) Mater Sci Eng A463:22
6. Iwahashi Y, Horita Z, Nemoto M, Langdon TG (1998) Metall Mater Trans 29A:2503
7. Prangnell PB, Hayes JS, Bowen JR, Apps PJ, Bate PS (2004) Acta Mater 52:3193
8. Morris DG, Muñoz-Morris MA (2002) Acta Mater 50:4047
9. Hughes DA (1993) Acta Metall Mater 41:1421
10. Zolotorevsky NYu, Solonin AN, Churyumov AYu, Zolotorevsky VS (2009) Mater Sci Eng A502:111
11. Nes E, Marthinsen K (2002) Mater Sci Eng A322:76
12. Schulthess TC, Turchia PEA, Gonisa A, Nieh T-G (1998) Acta Mater 46:2215
13. Murayama M, Horita Z, Hono K (2001) Acta Mater 49:21
14. Straumal B, Baretzky B, Mazilkin AA, Phillipp F, Kogtenkova OA, Volkov MN, Valiev RZ (2004) Acta Mater 52:4469
15. Zhao YH, Liao XZ, Jin Z, Valiev RZ, Zhu YT (2004) Acta Mater 52:4589
16. Segal VM (1999) Mater Sci Eng A 271:322
17. Aaron HB, Aaronson HA (1968) Acta Metall 16:789
18. Saunders N (2001) J JILM 51:141
19. Vaughan D (1968) Acta Metall 16:563
20. Russell KC (1969) Acta Metall 17:1123
21. Cantrell MA, Shiflet GJ (1994) Mater Res Soc Proc 319:351
22. Du Y, Chang YA, Huang B, Gong W, Jin Z, Xu H, Yuan Z, Liu Y, He Y, Xie F-Y (2003) Mater Sci Eng A363:140
23. Brailsford AD, Aaron HB (1969) J App Phys 40:1702
24. Lechner W, Puff W, Mingler B, Zehetbauer MJ, Würschu R (2009) Scripta Mater 61:383
25. Huang JY, Liao XZ, Zhu YT, Zhou F, Lavernia EJ (2003) Phil Mag 83:1407
26. Hutchinson CR, Gable BM, Ciccosillo N, Loo PT, Bastow TJ, Hill AJ (2008) In: Hirsch J, Skrotzki B, Gottstein G (eds) Aluminium alloys, ICAA 11. Wiley, p 788
27. Carolan RA, Faulkner RG (1988) Acta Metall 36:257